Supporting Information

Stoichiometric and electrocatalytic production of hydrogen peroxide driven by a water-soluble copper(II) complex

Hana Oh,[‡a] Suhyuk Choi,[‡b] Joo Yeon Kim,[b] Hyun S. Ahn*[b] and Seungwoo Hong*[a]

[a] *Department of Chemistry, Sookmyung Women's University, Seoul 04310, Korea.*

[b] *Department of Chemistry, Yonsei University, 50 Yonsei-ro, Seodaemun-gu, Seoul, 03722 Republic of Korea*

E-mail: ; hsw@sm.ac.kr and ahnhs@yonsei.ac.kr

Experimental Section

Materials and Instrumentation. Commercially available chemicals were used without further purification unless otherwise indicated. Solvents were dried according to published procedures and distilled under Ar prior to use.[S1] The nonheme copper(II) complex was prepared according to the literature methods.[S2] UV-vis spectra were recorded on a Hewlett Packard Agilent Cary 8454 UV-visible spectrophotometer equipped with a T2/sport temperature controlled cuvette holder. Electrospray ionization mass spectra (ESI MS) were collected on a Thermo Finnigan (San Jose, CA, USA) LTQ^{TM} XL ion trap instrument, by infusing samples directly into the source at 5.0 μL/min using a syringe pump. The spray voltage was set at 4.7 kV and the capillary temperature at 120 ^{o}C. Electrochemical measurements were performed on a CHI617B electrochemical analyzer (CH Instruments, Inc.) in CH_3CN containing 0.10 M Bu_4NPF_6 ($TBAPF_6$) as a supporting electrolyte at 25 ^{o}C. X-band EPR spectra were recorded at 77 K using an X-band Bruker EMX-plus spectrometer equipped with a dual mode cavity (ER 4116DM). Low temperatures were achieved and controlled with an Oxford Instruments ESR900 liquid He quartz cryostat with an Oxford Instruments ITC503 temperature and gas flow controller. A conventional three-electrode cell was used with a glassy carbon working electrode (surface area of 0.030 cm^2), a platinum wire as a counter electrode and an Ag/Ag^+ electrode as a reference electrode. The glassy carbon working electrode was routinely polished with BAS polishing alumina suspension and rinsed with acetone and acetonitrile before use. The measured potentials were recorded with respect to an Ag/Ag^+ (0.010 M) reference electrode. All potentials (vs Ag/Ag^+) were converted to values vs SCE by adding 0.29 V.[S3] Oxygen quantification experiments were performed on an Agilent 7890B gas chramatography instrument equipped with a thermal conductivity detector. Nitrogen was employed as a carrier gas and separation was done on a Supelco 60/80 Carboxen 1000 column. Oxygen quantification calibration curve is provided in Figure S14.

Synthesis and Characterization of Mono- and dinuclear Copper(II) and Copper(I) Complexes, 1, 2 and 3. The mononuclear copper(II) and copper(I) complexes bearing identical HN3O2 ligand, $[Cu^{II}(HN3O2)(H_2O)](ClO_4)_2$ (**1**), and $[Cu^{I}(HN3O2)]^+$ (**2**), were prepared by reacting HN3O2 ligand and equimolar of $Cu(ClO_4)_2{\cdot}6H_2O$ for **1** and equimolar

of CuI for **2**, respectively, in CH_3CN. The UV-vis spectrum of **1** exhibited characteristic d-d band at 615 nm whereas **2** showed an intensive band at around 300 nm, respectively.The dicopper(II) complex, $[Cu_2^{II}(O_2)(HN3O2)_2]^{2+}$ (**3**), was obtained by reacting **2** and O_2 in CH_3CN at 20 °C.

X-Ray Structural Analysis. Single crystals of copper(II) complex suitable for X-ray crystallographic analysis were obtained by slow diffusion of Et_2O into a EtOH solution of **1**. These crystals were taken from the solutions by a nylon loop (Hampton Research Co.) on a hand made cooper plate and mounted on a goniometer head in a N_2 cryostream. The diffraction data for **1** was collected at 120 K on a Bruker SMART AXS diffractometer equipped with a monochromator in the Mo *K*α (λ = 0.71073 Å) incident beam. Cell parameters were determined and refined by the SMART program.[S4] The CCD data were integrated and scaled using the Bruker-SAINT software package.[S5] An empirical absorption correction was applied using the SADABS program.[S6] The structures were solved by direct methods, and all non-hydrogen atoms were subjected to anisotropic refinement by full-matrix least squares on F^2 by using SHELXTL Ver. 6.14.[S7] The crystallographic data and selected bond distances and angles are listed in Tables S1 and S2, respectively. Full crystallographic details can be obtained free of charge from the Cambridge Crystallographic Data Centre via www.ccdc.cam.ac.uk/data_request/cif (CCDC 1923352).

Iodometric Titration Experiment. The quantity of H_2O_2 formed in the O_2 reduction reaction was determined by iodometic titration. To an O_2-saturated CH_3CN solution of **1** (0.010 mM), $HClO_4$ (0.050 mM) and Me_8Fc (0.050 mM) were added sequentially at 25 °C. Prompt formation of Me_8Fc^+ (λ_{max} = 750 nm, ε = 400 M^{-1} cm^{-1}) can be observed by UV-vis spectroscopy. The reaction solution was then treated by an excess of NaI (20 mM). The formation of I_3^- was detected at 360 nm ($\varepsilon = 2.8 \times 10^4$ M^{-1} cm^{-1}) due to the presence of H_2O_2; the amount of I_3^- was quantified based on its extinction coefficient.

Reactivity Studies. Kinetic measurements were performed on a Hewlett Packard 8453 photodiode-array spectrophotometer for O_2 activation reaction by **2** to **3** in CH_3CN at 20 °C. Reactions were run in a 1.0 cm UV cuvette, monitoring UV−vis spectral changes of reaction

solutions. Rate constants were determined under pseudo-first-order conditions (e.g., [substrate]/[**2**] > 10) by fitting the absorbance changes at 650 nm due to **2**. Fast reaction traces were collected using a 1.0 cm optical path length of stopped-flow cell. For the reduction reaction of **1** to **2**, the time dependence of the absorbance at 750 nm due to the formation of octamethylferrocenium ion was fitted with single exponential function to give k_{obs} (s^{-1}) under the pseudo-first-order conditions in CH_3CN at 20 °C. For the protonation reaction of peroxide ligand within **3**, the time dependence of the absorbance at 650 nm due to the decay of **3** was fitted with single exponential function to give k_{obs} (s^{-1}) under the pseudo-first-order conditions in CH_3CN at 20 °C. The raw kinetic data were treated with KinetAsyst 3 (Hi-Tech Scientific) and Specfit/32 Global Analysis System software from Spectrum Software Associates. The kinetic experiments were run at least in triplicate, and the data reported represent the average of these reactions.

Electrocatalytic Oxygen Reduction Reaction (ORR). All the oxygen reduction catalysis experiments were progressed in an O_2-saturated 0.10 M phosphate buffered (pH 10) solution containing **1** (0.20 mM) with 0.90 M KNO_3 supporting electrolyte at 20 °C. Linear Sweep Voltammetry (LSV) experiments used conventional three electrode cell with a 5.0 mm glassy carbon RDE, Pt wire counter electrode, and a Ag/AgCl, 1.0 M KCl reference electrode.

DFT Calculations. The energy-minimized geometric structure of **3** was obtained by Gaussian 09. The B3LYP density functional in 6-311G(d,p) level was used for main elements (C,H,N,O), whereas B3LYP/LANL2DZ/ECP basis set was used for Cu. In energy calculations, time-dependent DFT (TD-DFT) was conducted to gain singlet excited states of **3**. The solvent effect of the conductor-like polarizable continuum model (CPCM) with acetonitrile (ε = 35.688) was applied to all calculations.

Table S1. Crystallographic Data and Refinements for **1**

	1
Empirical formula	$C_{16}H_{23}Cl_2CuN_3O_{11}$
Formula weight	567.81
Temperature (K)	120
Wavelength (Å)	0.71073
Crystal system/space group	monoclinic, $P_{21/c}$
Unit cell dimensions	
a (Å)	9.349(3)
b (Å)	11.095(3)
c (Å)	21.794(6)
α (°)	90
bβ (°)	100.37(3)
γ (°)	90
Volume (Å^3)	2224.0(10)
Z	4
Calculated density (g/cm^{-3})	1.696
Absorption coefficient (mm^{-1})	1.286
Reflections collected	3919
Absorption correction	multi-scan (T_{min} = 0.468, T_{max}= 0.745)
Independent reflections	3079
Goodness-of-fit on F^2	1.069
R [F^2 > 2sigma(F^2)]	0.0542
wR^2	0.1533

Table S2. Selected Bond Distances (Å) and Angles (°) for **1**

	1
Bond Distances (Å)	
Cu1-N1	1.973(4)
Cu1-N2	2.020(3)
Cu1-N3	1.980(3)
Cu1-O1	1.958(3)
Cu1-O2’	2.402(3)
Bond Angles (°)	
N1-Cu1-N2	83.64(14)
N1-Cu1-N3	166.16(14)
N2- Cu1-N3	83.29(14)
N1- Cu1-O1	93.60(14)
N2-Cu1-O1	174.28(14)
N3-Cu1-O1	99.81(14)
N1-Cu1-O2	88.24(12)
N2-Cu1-O2	81.39(11)
N3-Cu1-O2	94.30(12)

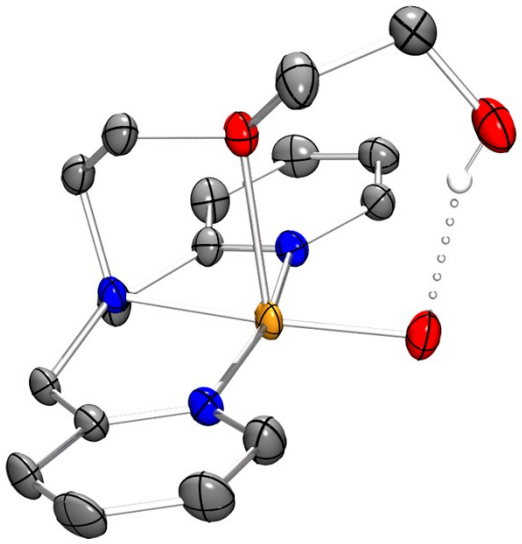

Fig. S1 Crystal structure of $[Cu^{II}(HN3O2)(H_2O)](ClO_4)_2$ (**1**), with thermal ellipsoids showing 50% probability. Two perchlorate ions are omitted for clarity (see Table S1 and S2).

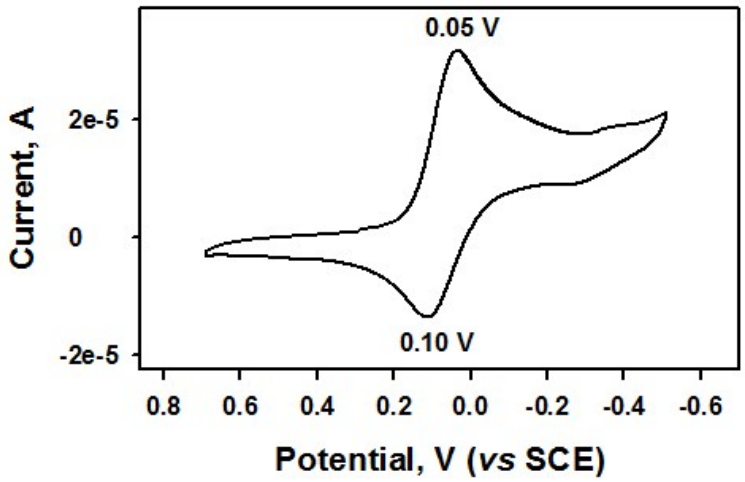

Fig. S2 Cyclic voltammogram of **1** (1.0 mM) in CH_3CN containing $TBAPF_6$ (0.10 M) with a glassy carbon working electrode at 298 K. Scan rate was 0.10 V s^{-1}.

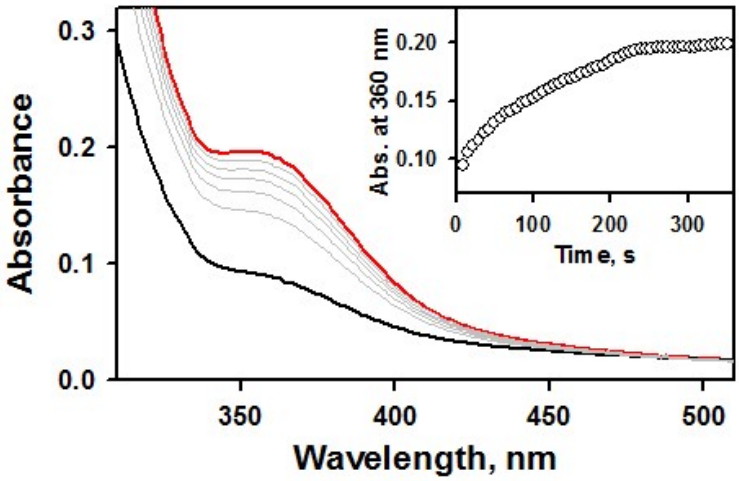

Fig. S3 UV-vis spectral changes obtained upon addition of NaI (20 mM, red line) into the reaction solution containing **1** (0.010 mM, black line) in the presence of $HClO_4$ (0.050 mM) and Me_8Fc (0.050 mM) in CH_3CN at 20 ^oC.

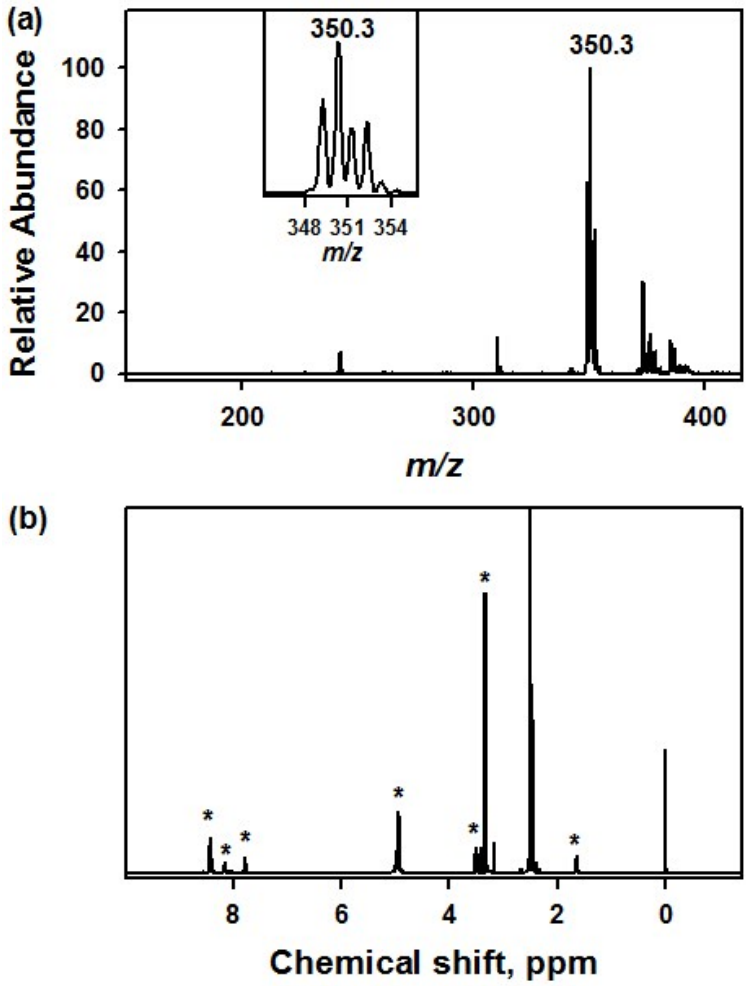

Fig. S4 (a) ESI MS spectrum of **2** recorded in CH_3CN. The prominent ion peak at *m/z* of 350.3 correspond to $[Cu^{I}(HN3O2)]^{+}$ (calculated *m/z* of 350.1). Inset shows the mixed isotopic distribution pattern of $[Cu^{I}(HN3O2)]^{+}$ and $[Cu^{II}(N3O2)]^{+}$ (calculated *m/z* of 349.1) due to the instability of **2** under air. (b) Diamagnetic ^{1}H NMR spectrum of **2** in DMSO at 25 ^{o}C. * show the HN3O2 ligand peak.

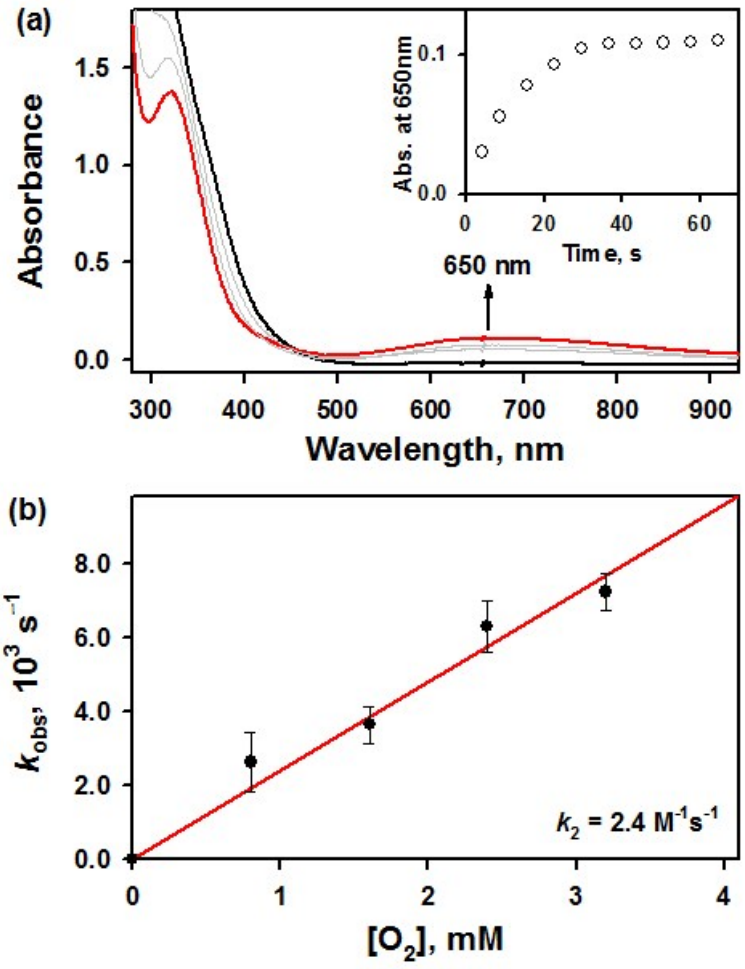

Fig. S5 (a) UV-Vis spectral changes observed in the reaction of **2** (1.0 mM) and excess O_2 in O_2-saturated CH_3CN at 20 °C. Inset shows the time courses monitored at 650 nm due to the formation of **3**. (b) Plot of pseudo-first-order rate constants (k_{obs}) against the concentration of O_2 to determine a second-order rate constant in the reaction between **2** (1.0 mM) and O_2 in CH_3CN at 20 °C.

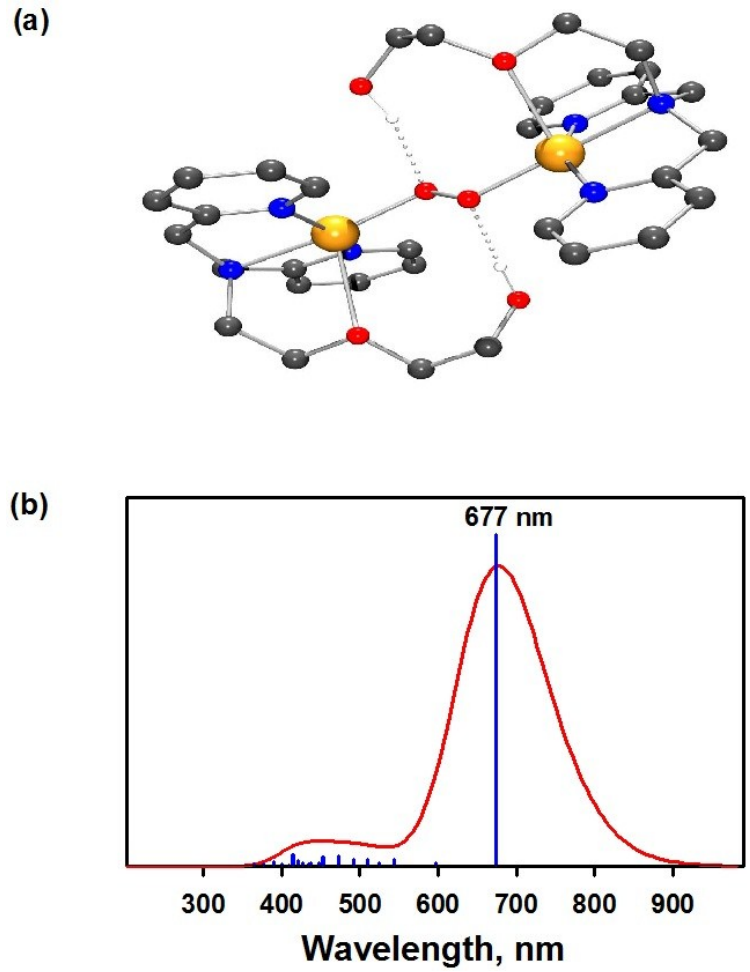

Fig. S6 (a) DFT-optimized structure of **3** and (b) TD-DFT calculated theoretical excitation energies of **3**.

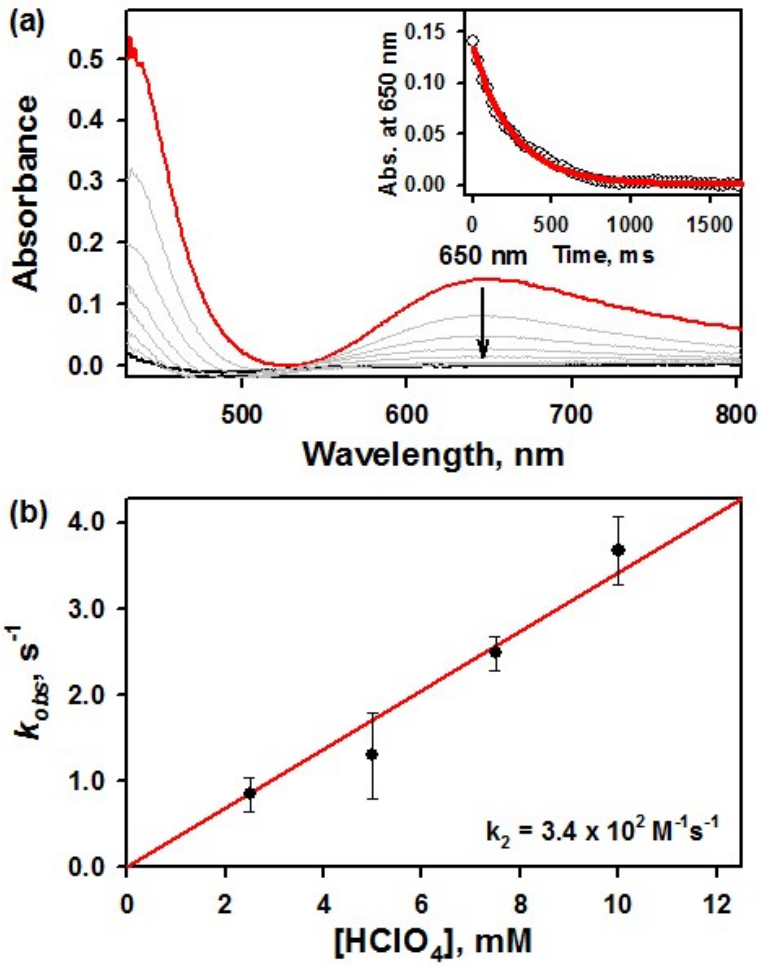

Fig. S7 (a) UV-Vis spectral changes observed in the reaction of **3** (1.0 mM) and $HClO_4$ (5.0 mM) in O_2-saturated CH_3CN at 20 °C. Inset shows the time courses monitored at 650 nm due to the decay of **3**. (b) Plot of pseudo-first-order rate constants (k_{obs}) against the concentration of O_2 to determine a second-order rate constant in the reaction between **2** (1.0 mM) and O_2 in CH_3CN at 20 °C.

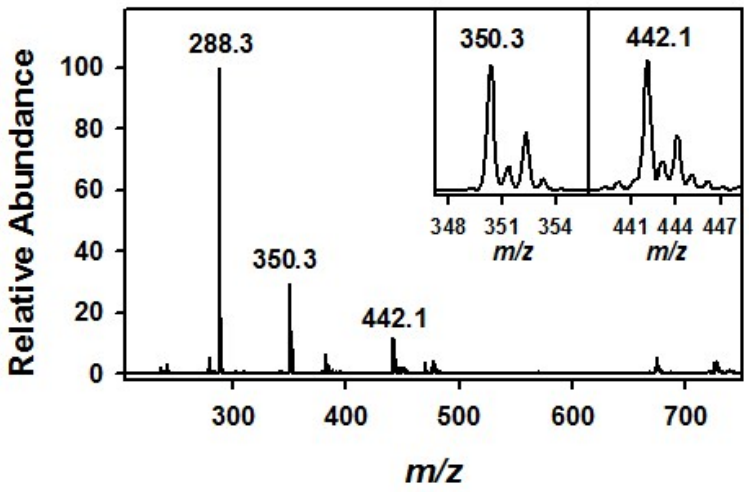

Fig. S8 ESI MS spectrum obtained in the reaction of **3** (1.0 mM) and $HClO_4$ (1.0 mM) recorded in CH_3CN. The peak at *m*/*z* = 288.3 correspond to protonated $[HN3O2+H^+]^+$ (calculated *m*/*z* of 288.2) and the peak at *m*/*z* = 350.3 and 442.1 correspond to $[Cu^{I}(HN3O2)]^+$ (calculated *m*/*z* of 350.1) and $[Cu^{II}(HN3O2)(CH_3CN)(CH_3O)]^+$ (calculated *m*/*z* of 422.1), respectively. Insets show the observed isotope distribution patterns for $[Cu^{II}(HN3O2)]^+$ and $[Cu^{I}(HN3O2)(CH_3CN)(CH_3O)]^+$, respectively.

Production and accumulation of oxidative H_2O_2 experiment. The production and accumulation of H_2O_2 were performed using a two-compartment cell equipped with an AHA (ASTOM Corporation, Tokyo, Japan) as an anion-exchange membrane between the anode and cathode. The cell was kept in an ice bath and away from light via an aluminum foil cover throughout the experiment. Calibration curve for the iodometric detection of H_2O_2 is shown below.

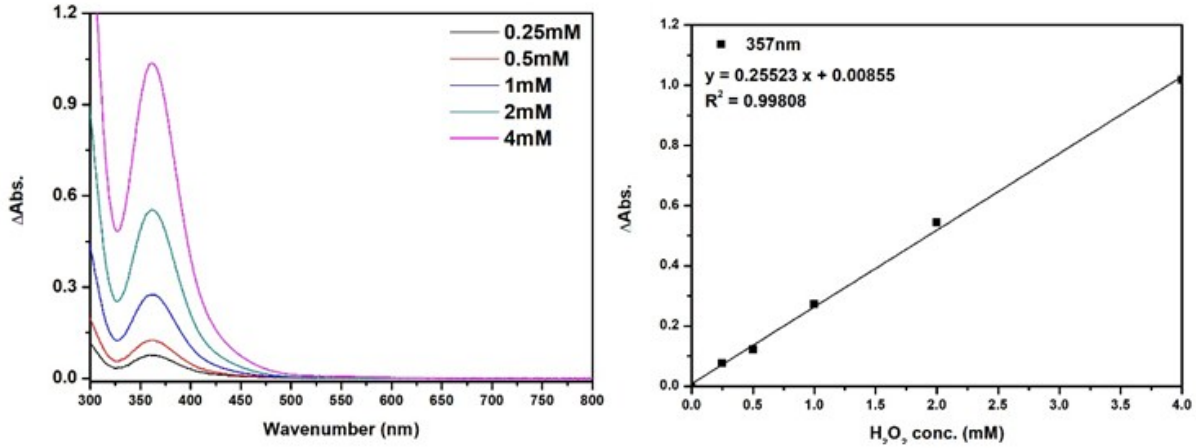

Fig. S9 UV-vis absorption spectra of various concentrations of H_2O_2 in an iodometric titration (left) and the resulting calibration curve (right).

Koutecky-Levich Analysis of the Oxygen Reduction Reaction Employing 1 as a Catalyst

The Koutecky-Levich equation provides important insight about the electron transfer reaction when all other variables are controlled and the rotation rate (convection mass transport) of the electrode is the only variable.[S8] The equation is shown below:

$$\mathbf{i = (0.620)}\, nFAD^{\frac{2}{3}}\omega^{\frac{1}{2}}\nu^{\frac{-1}{6}}C$$

where n is the number of electrons transferred (in this case 2 for H_2O_2 production and 4 for water generation), F is the Faraday's constant, D is the diffusion coefficient of the analyte (dioxygen), ω is the rotation rate of the electrode, υ is the viscosity of the solvent, and C is the concentration of dissolved O_2 in water. When the inverse of current is plotted against the inverse of the rotation rate, the electron transfer number n can be obtained from the slope and shed insight as to the H_2O_2 selectivity over four electron reduction to water.

In the case of ORR electrocatalysis by **1**, the following Levich plot was obtained, with n = 2.9, indicating that the H_2O_2 selectivity was 55 %.

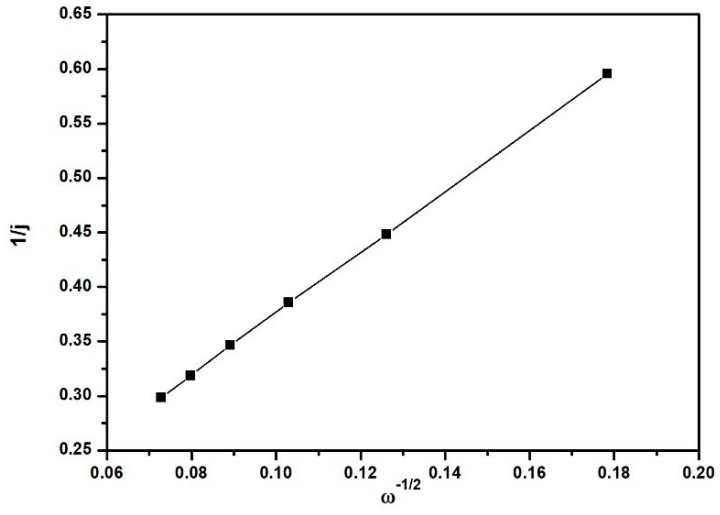

Fig. S10 Levich plot of ORR electrocatalyses by compound **1**. From the slope, n was determined to be 2.9.

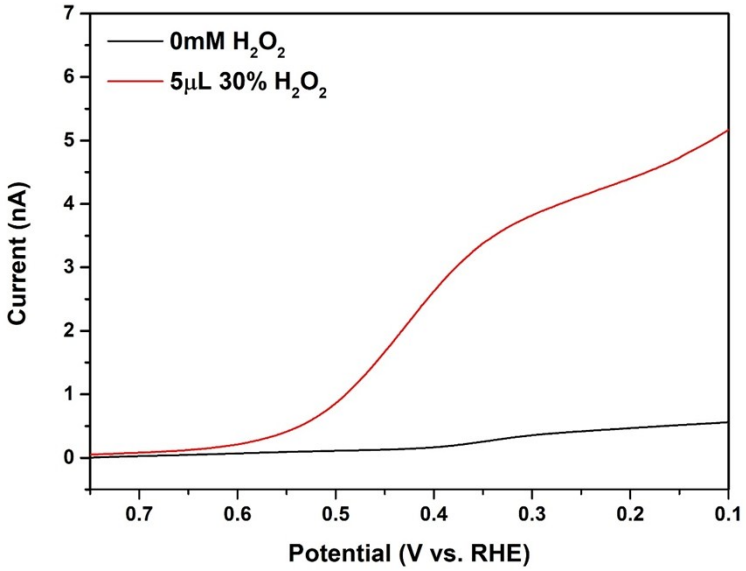

Fig. S11 Linear sweep voltammetry of a glassy carbon electrode in the absence (black trace) and in the presence (red trace) of H_2O_2 at reducing potentials. H_2O_2 reduction to water was observed at potentials more negative than 0.50 V. At ORR potentials for compound **1** (more negative than 0.30 V), H_2O_2 produced by **1** was further reduced to water by bare glassy carbon electrode, and therefore, accumulation of H_2O_2 at ORR potentials was not possible.plot of ORR electrocatalyses by compound **1**.

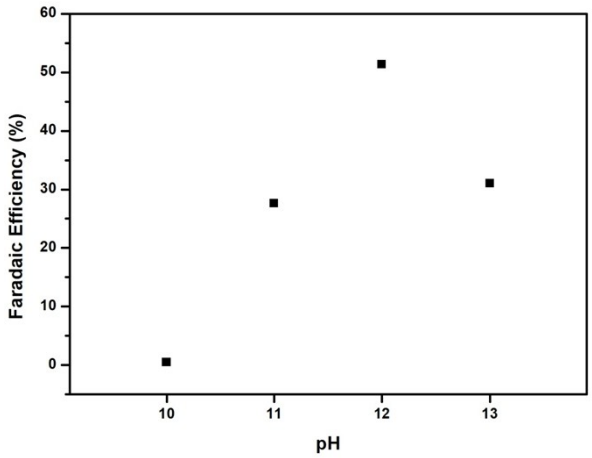

Fig. S12 The plot of maximum Faradaic efficiencies for H_2O_2 production during water oxidation by compound **1** at pHs 10 to 13. Negligible selectivity was observed at pH 10, and the maximum of 51 % was obtained at pH 12.

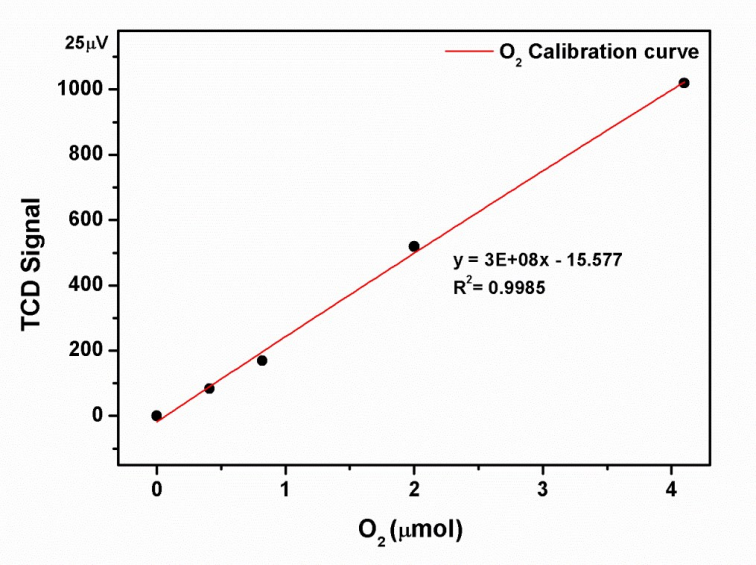

Fig. S13 Oxygen quantification calibration curve by gas chromatography thermal conductivity detector.

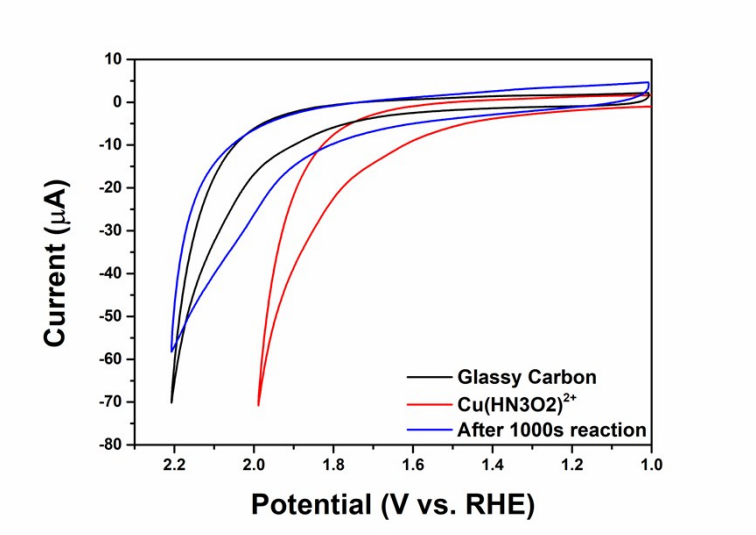

Fig. S14 Oxygen evolution cyclic voltammograms in pH 12 water of a bare glassy carbon (black trace), that with $Cu(HN3O2)^{2+}$ (red trace), and that after running the reaction for 1000 s (blue trace). The blue trace is that of a rinse test, where the glassy carbon employed for catalysis with a copper compound for 1000 s was isolated, rinsed with deionized water, and then placed in a pH 12 solution without the copper catalyst and evaluated electrochemically. The results suggest that slight physisorption occurred without significant amount of copper compound degradation. With gentle sonication and continued rinsing, the electrode that produced the blue trace reverted back to one with a voltammogram superimposable on the black trace without mechanical polishing, further suggesting that the nature of adsorption is weak physisorption. Other sets of electrodes used in the catalysis with varying degrees of involvement (from as short as 60 s to as long as 6000 s) displayed similar behavior.

Cartesian Coordinates

Coordinates for optimized **3**

Cu	-2.3371	-0.0367	0.2414	H	-4.5123	-2.3301	-0.4503	C	1.5951	4.2278	0.8331
O	-3.0807	-0.8893	-2.073	H	-5.3985	-1.8043	1.9196	C	4.8449	1.7487	-0.3684
N	-3.0808	1.7729	-0.3147	H	-4.3975	-0.5373	2.6256	C	1.2767	0.5465	3.637
N	-2.1413	-1.7655	1.2887	H	-6.1328	3.1669	-0.4193	O	-0.0117	0.5193	3.0344
N	-4.4427	-0.4819	0.5287	H	-0.0847	-4.2824	2.1189	H	0.0437	0.5363	2.0637
C	-3.2762	-2.1805	1.8851	H	-0.157	-2.1056	0.8762	H	0.4676	2.4161	0.4652
C	-2.3783	2.7315	-0.9375	H	-2.3674	4.652	-1.8879	H	3.0439	5.7974	1.1286
C	-4.337	4.0727	-1.2007	H	-6.1671	0.7506	0.2586	H	4.1585	-4.8182	-2.9813
C	-2.1693	-4.1528	2.6836	H	-5.1836	1.119	1.6644	H	5.6942	-2.9049	-2.526
C	-3.3223	-3.3795	2.5877	H	-3.1515	-1.2529	-4.1066	H	4.7026	-0.4257	3.0834
C	-4.5015	-0.8409	-1.968	H	-2.899	0.4504	-3.654	H	4.1755	1.1173	2.3965
C	-4.9217	-1.3291	-0.5953	H	-0.8687	-1.7716	-3.1474	H	6.0766	-0.0259	1.1528
C	-4.4642	-1.2462	1.7967	H	-0.918	-0.7919	-4.617	H	4.9954	-1.3949	0.8592
C	-5.065	3.0702	-0.5702	Cu	2.3655	0.1162	-0.3088	H	6.0498	-0.744	-1.3633
C	-4.405	1.9242	-0.134	O	2.9003	-0.5045	2.0586	H	4.895	0.1667	-2.3325
C	-1.0014	-3.71	2.0697	N	2.472	2.1219	0.1164	H	4.9637	4.3433	0.4828
C	-1.0303	-2.5072	1.3774	N	2.8437	-1.6012	-1.3208	H	1.7422	-4.6046	-2.3399
C	-2.9679	3.9014	-1.3914	N	4.5342	0.3064	-0.2723	H	0.9852	-2.4866	-1.257
C	-5.1343	0.8243	0.6136	C	4.1405	-1.6971	-1.67	H	0.7309	4.8174	1.1086
C	-2.6365	-0.5853	-3.403	C	1.4391	2.8986	0.4704	H	5.7664	1.9915	0.1702
C	-1.1394	-0.7864	-3.5449	C	2.8792	4.7662	0.8408	H	5.0235	1.9953	-1.4177
O	-0.3607	0.2453	-2.9533	C	3.7852	-3.913	-2.5181	H	1.0971	0.5268	4.7151
H	-0.0986	-0.0196	-2.053	C	4.6449	-2.8488	-2.2657	H	1.8085	1.4806	3.4114
H	-1.3255	2.525	-1.0747	C	4.2135	0.0363	2.2187	C	2.1602	-0.6479	3.2856
H	-4.8332	4.971	-1.5475	C	5.0305	-0.3119	0.987	H	1.5329	-1.5337	3.1659
H	-2.1851	-5.0904	3.2258	C	4.9937	-0.4669	-1.4481	H	2.869	-0.8384	4.0987
H	-4.2487	-3.6984	3.0481	C	3.9514	3.9588	0.4812	O	0.4342	-0.321	-0.3475
H	-4.9528	-1.5072	-2.7133	C	3.7161	2.6358	0.1145	O	-0.4391	0.5423	0.2171
H	-4.8645	0.1741	-2.172	C	2.4441	-3.8008	-2.1626				
H	-6.0158	-1.4067	-0.5615	C	2.0152	-2.6268	-1.56				

References

[S1] W. L. F. Armarego and C. L. L. Chai, *Purification of Laboratory Chemicals,* 6th ed.; Pergamon Press: Oxford, 2009.

[S2] S. J. Kirin, C. M. Happel, S. Hrubanova, T. Weyermüller, C. Klein and N. Metzler-Nolte, *Dalton Trans.,* 2014, 1201

[S3] C. K. Mann and K. K. Barnes, in *Electrochemical Reactions in Non-aqueous Systems*, Mercel Dekker, New York, 1970.

[S4] *SMART*, Data collection software; Bruker AXS Inc.: Madison, Wisconsin, USA, 2012.

[S5] *SAINT*, Data integration software; Bruker AXS, Inc.: Madison, Wisconsin, USA, 2012.

[S6] Sheldrick, G. M. *SADABS*, Program for absorption correction with the Bruker SMART system; Universität Göttingen, Germany, 1996.

[S7] Sheldrick, G. M. *SHELXTL*, *Version 6.14*; Bruker AXS Inc.: Madison, Wisconsin, USA, 2003.

[S8] A. J. Bard and L. R. Faulkner, Electrochemical Methods: Fundamentals and Applications, John Wiley & Sons, New York, 2011.